Earth and Planetary Science Letters 554 (2021) 116671

Contents lists available at ScienceDirect

Earth and Planetary Science Letters

www.elsevier.com/locate/epsl

Overspilling small craters on a dry Mars: Insights from breach erosion modeling

A.O. Warren [a,*], S. Holo [a], E.S. Kite [a], S.A. Wilson [b]

[a] University of Chicago, Chicago, IL 6063, USA
[b] Center for Earth and Planetary Studies, National Air and Space Museum, Smithsonian Institution, 6th at Independence SW, Washington, DC 20560, USA

ARTICLE INFO

Article history:
Received 20 July 2020
Received in revised form 21 October 2020
Accepted 7 November 2020
Available online 19 November 2020
Editor: W.B. McKinnon

Keywords:
planetary science
Mars
sediment transport

ABSTRACT

Understanding when, where, and how frequently liquid water was stable on Mars since the Late Noachian/Early Hesperian (3.2-3.9 Ga) is important for understanding the evolution of Mars' climate and hydrology. Some relatively young features on Mars require multiple wetting events to form, whereas others are consistent with single wetting events. Small and rare exit breach craters or "pollywogs" are craters between 0.5 and 15 km in diameter with valleys leading away from the lowest point on their rims but no visible inlet valleys. These craters must have been filled with water to the point of overspill to form the observed valleys. The two possible water sources are precipitation and groundwater. In this paper we use measurements from Digital Elevation Models (DEMs) of 18 pollywog craters (21 outlet valleys) and a fixed channel width 0-D breach erosion model to determine whether pollywog exit breach valleys are consistent with a single crater overspill event, or if their formation requires multiple overspill events. Our model, which we compare to a selection of dam breaching events on Earth, predicts runaway erosion for two pollywog exit breaches. No runaway erosion is observed. We discuss potential explanations for this mismatch between the data and our model. We show that the majority of pollywog craters on Mars are consistent with formation during a single crater overspill event, incorporating a work around for the long-standing problem of unknown grainsize into our approach. Three pollywog craters require either multiple events or sustained water supply to drive erosion. We discuss potential source mechanisms for crater-filling water and conclude that pollywogs either formed in a single erosion event, driven by groundwater discharge, or through many small erosion events, driven by draining of small meltwater lakes formed on crater-filling bodies of ice.

1. Introduction

Surface liquid water on Mars requires conditions very different from the present day; either temperatures >273 K resulting from different climate conditions, or transport of water out of the subsurface for example by groundwater outflows (Rodriguez et al., 2015). If the water source is known, morphological features (e.g. fluvial channels, lake deposits) can be used to understand either the evolution of the Martian climate and atmosphere, or the evolution of the hydrosphere. Wet events on Mars since the Valley Network forming period (<3.2-3.9 Ga) (Hartmann, 2005) are recorded by the formation of features such as alluvial fans (Kite et al., 2019; Hauber et al., 2013), and small exit breach craters or "pollywogs" (Wilson et al., 2016). These features indicate a trend from an earlier, wetter climate with intense fluvial erosion (Matsubara et al., 2013), to arid conditions punctuated by occasional surface liquid water (Kite et al., 2019). Pollywogs have outlet valleys extending from well-preserved crater rims, but no inlet valleys (Wilson et al., 2016) e.g. Fig. 1a. The outlet valleys formed by overspill of water from within the crater. Fresh pollywog rims indicate that pollywog outlet incision post-dates the intense Late Noachian and Early Hesperian fluvial activity (Wilson et al., 2016). Pollywog formation requires a water source that left crater rims intact, but was intense enough to supply $>10^7$ m^3 of water under dry climate conditions. Two possible sources of this water are groundwater (e.g. from a pressurized aquifer at depth), and precipitation and/or melting (Fig. 2). If erosion during a single pollywog overspill event can be constrained, then the observed erosion from pollywog overspill events is an important constraint on the number, duration, and intensity of mid-latitude surface liquid water events on Mars since the Late Noachian/Early Hesperian (3.9-3.2 Ga) (Hartmann, 2005).

Low-latitude alluvial fans require multiple episodes of wetting (Hauber et al., 2013; Kite et al., 2019). Groundwater modeling has

* Corresponding author.
E-mail address: aowarren@uchicago.edu (A.O. Warren).

https://doi.org/10.1016/j.epsl.2020.116671
0012-821X/

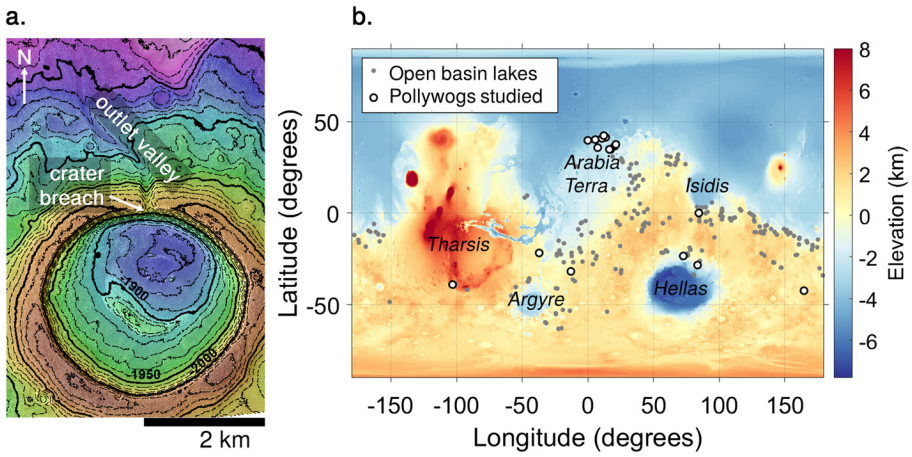

Fig. 1. a. Pollywog HiRISE DEM centered at 34.797°N 17.398°E (ESP_053222_2150/ESP_052945_2150) overlain on orthophoto. Elevations relative to Mars geoid. Thick contour spacing is 50 m. Thin, dashed contour spacing is 10 m. b. Topographic map of Mars showing locations of Digital Elevation Models (DEMs) of exit breach craters (pollywogs) used in this study (Table 1) and Valley Network-fed open basin lakes (i.e. lakes with outlet valleys) (Fassett and Head, 2008) for comparison with older, climate-driven Noachian features. Topography data comes from the Mars Orbiter Laser Altimeter (MOLA). (For interpretation of the colors in the figure(s), the reader is referred to the web version of this article.)

shown that outflow channel formation may be more consistent with multiple, smaller-magnitude groundwater discharge events than a single flood (Andrews-Hanna and Phillips, 2007). However, other features are consistent with a single wet event, for example impact-driven melting and precipitation in Mojave and Hale craters (Goddard et al., 2014). Do pollywogs belong to the first group of features (Gale, alluvial fans) that record signatures of global climate conditions during the Hesperian? Or do they result from localized groundwater or impact-induced conditions?

Global climate and local conditions are plausible explanations for pollywogs. Accumulating sufficient surface liquid water to overspill a pollywog through precipitation and snowmelt is challenging in a climate that is consistent with low erosion rates (Golombek et al., 2006) and valley distributions and morphologies consistent with reduced precipitation rates relative to the Noachian (>3.6-3.7 Ga) (Harrison and Grimm, 2005). Models of Martian climate under different orbital conditions can produce ice accumulation in midlatitudes (Mischna et al., 2013), and some melting (Kite et al., 2013). This makes ice-filled craters with melt ponds on their surfaces a plausible watersource for pollywog outlet valley erosion (e.g. Fig. 2). Orbital changes provide a potential mechanism for pacing surface liquid water activity (Jakosky et al., 1995). Large impacts (Steakley et al., 2019; Turbet et al., 2020) may also be able to induce short-lived climates enabling surface liquid water. Groundwater discharge from pressurized aquifers is an alternative mechanism for supplying liquid water to the surface during the Hesperian (Andrews-Hanna and Phillips, 2007; Rodriguez et al., 2015), e.g. in Xanthe Terra (Coleman, 2005), and some large (D >30 km) crater lake breach valleys (Warner et al., 2010).

The expected valley floor erosion from a single pollywog overspill event compared with observed erosion depths is an important constraint on Mars' climate and hydrology since the Late Noachian/Early Hesperian (Fig. 1a) because it can be used to infer the properties of the pollywog-overspilling water source. In this paper, we determine whether pollywog exit breach valleys are consistent with a single overspill event, or if their formation requires multiple overspill events. We use a new fixed channel width 0-D model (Section 2.1) and pollywog measurements from HiRISE Digital Elevation Models (DEMs) (Section 3.1) to predict the erosion that can occur in a single crater overspill event. The model is ground-truthed using terrestrial dam breach flood data (Section 3.2). We compare model predictions and observed breaches (Section 4), and consider the climate and hydrological conditions under which all studied pollywogs could be consistent with a single overspill event (Section 5).

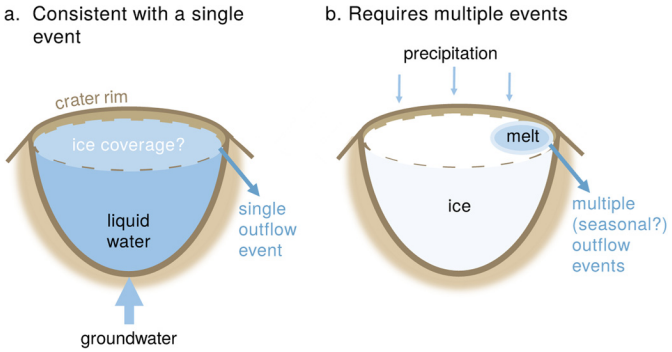

Fig. 2. Schematic illustration of preferred pollywog overspill mechanisms. a. Crater fills and overspills during a single groundwater discharge event. $Q_{in} > 0$ is required for some craters (Section 5). b. Crater fills gradually with ice. Favorable climate conditions enable a melt pond/annulus smaller than the crater to form, which drains over the crater rim, contributing a small amount of erosion per overspill event. This mechanism repeats until the full breach depth is eroded.

2. Methods

In Section 2.1 we describe our new model for breach erosion. In Section 3.1 we describe our pollywog measurements, their implications, and how they are used in the breach erosion model. In Section 3.2 we test the model against terrestrial exit breach erosion events.

2.1. Breach erosion model

Previous studies of crater overspill erosion on Mars (Goudge et al., 2019) have adapted models of terrestrial flooding, e.g. dam failure and weir flow (Walder and O'Connor, 1997). These models work well for flow breaching small barriers within a pre-existing channel (Morris et al., 2009; Walder and O'Connor, 1997). However, when the dam (the crater rim for pollywogs) extends for a greater distance down the valley, the cross section of the newly eroded channel restricts the flow of water downstream, affecting how the channel cross section varies over time through erosion (Morris et al., 2009). This is important for erosion into crater ejecta with no pre-existing valley. We used a new fixed channel width 0-

Table 1
Table of DEM numbers and locations (Fig. 1). Latitude and longitude give center of left HiRISE observation. Error estimates are standard deviations of diameter (D) measurements. DEMs made using University of Chicago HiRISE pipeline.

Breach		DEM (left image)	Lat (°N)	Long (°E)	Diameter, D (km)
1		ESP_049860_2160	35.800	7.546	10.1 ± 0.20
2		ESP_053367_2220	41.438	13.633	1.8 ± 0.04
3		ESP_055330_1565	−23.410	72.793	0.7 ± 0.01
4		ESP_061037_1375	−42.399	164.775	9.6 ± 0.31
5		ESP_061782_1480	−31.851	−12.883	10.9 ± 0.24
6		ESP_052112_1800	0.096	84.656	11.2 ± 0.37
7		ESP_053169_2170	36.703	20.651	5.6 ± 0.06
8		ESP_055147_2170	36.683	20.538	4.2 ± 0.07
9		ESP_055266_2210	40.887	10.838	3.8 ± 0.09
10		ESP_059541_1580	−21.751	−37.027	2.5 ± 0.05
11		ESP_034014_1405	−39.052	−103.026	10.4 ± 0.33
12		ESP_052945_2150	34.797	17.398	3.6 ± 0.10
13	a	ESP_053736_2180	37.573	21.404	6.3 ± 0.37
	b				6.3 ± 0.37
	c				6.3 ± 0.37
14	a	ESP_052510_2150	34.841	16.476	3.8 ± 0.19
	b				3.8 ± 0.19
15		ESP_062045_2200	39.794	0.035	2.3 ± 0.09
16		ESP_050585_2225	42.385	12.184	6.3 ± 0.22
17		ESP_061715_2205	40.199	5.687	0.4 ± 0.02
18		ESP_059352_1515	−28.399	83.651	0.7 ± 0.02

D model, adapted from Holo and Kite (2019), to investigate breach erosion processes.

Our model couples lake drainage to breach erosion by combining conservation of mass, and equations for flow resistance and transport-limited erosion. We assume no downstream changes in channel/valley geometry, flow depth, or flow velocity. We also assume that all sediment eroded is advected perfectly downstream and removed from the system, i.e. there is no modification of the flow through re-deposition. The elevation head (J) available to drive outflow and erosion in the pollywog channel is given by the difference between lake level (E), and breach floor elevation (B) (Fig. 3):

$$J = E - B \tag{1}$$

During lake draining, water accelerates from negligible velocity within the lake to a higher velocity at the breach. This causes drawdown of the lake level near the breach, so the flow depth at the breach (H) is less than the elevation head (J). Assuming critical flow at the breach, and a rectangular breach and channel, conservation of energy (French, 1985) gives:

$$H = \frac{2}{3}J \tag{2}$$

We assume that outlet channel flow depth and breach flow depth are equal, and use H to calculate both lake drainage and channel floor erosion.

We select a value of initial flow depth $1 < H < 10$ m for each model run. E is controlled by the water flux into (Q_{in}) and out of the lake (q_{out}). B is controlled by downwards erosion of the valley floor, which is controlled by the sediment flux (q_s) out of the channel per unit length (L). Our model assumes that $H \ll w_v$. All of q_s/L contributes to deepening the channel through erosion. Differentiating Eq. (1) gives:

$$\frac{dJ}{dt} = \frac{dE}{dt} - \frac{dB}{dt} \tag{3}$$

Where:

$$\frac{dE}{dt} = \frac{4(Q_{in} - w_c q_{out})}{\pi D^2} \tag{4}$$

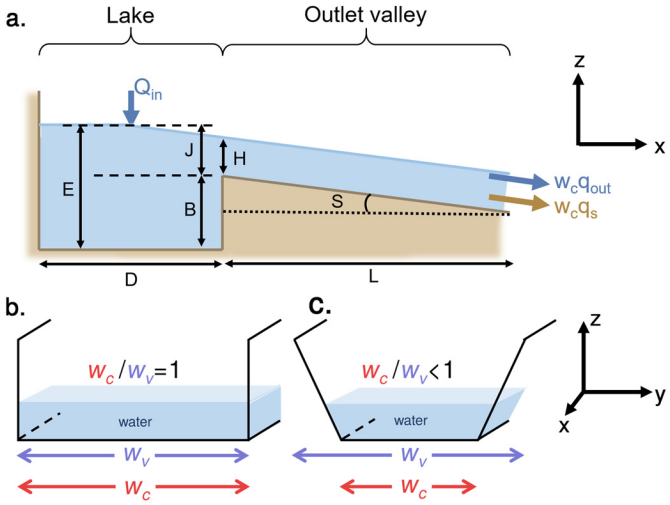

Fig. 3. a. Schematic illustration of crater breach erosion model. E is water level in the lake. B is breach floor elevation. J is the difference in elevation between lake level and the channel floor, also known as the elevation head. H is the water depth in the channel. L is channel length, D is lake diameter, S is channel slope, w_v is valley width, w_c is channel width, q_{out} is flow of water out of the crater, q_s is sediment flux out of the channel, and Q_{in} is flux of water into the crater. b. Rectangular trough shaped channel with $w_c = w_v$. This is assumed in all models in this study. c. Trapezoidal channel with $w_c < w_v$. This shape favors runaway erosion.

$$\frac{dB}{dt} = -\left(\frac{w_c}{w_v}\right)\frac{q_s}{L} \tag{5}$$

Using Manning's Law for water discharge in a channel:

$$q_{out} = \frac{H^{5/3}S^{1/2}}{n} \tag{6}$$

And a standard scaling for Manning's n (Brownlie, 1983):

$$n = \frac{k^{1/6}}{8g^{1/2}} \tag{7}$$

where k is the channel bed roughness lengthscale. In alluvial channels, k is typically larger than grainsize d (Kamphuis, 1974). The k used depends on whether d represents the grainsize for which 50% of grains are smaller (for d_{50}, $k = 2.5d_{50}$), or 90% of grains are smaller (for d_{90}, two common approximations are $k = d_{90}$ and $k = 3d_{90}$) (Van Rijn, 1984). We assume a uniform grainsize ($d_{50} = d_{90}$) and $k = d$ because $k > d$ disfavors erosion, therefore assuming $k = d$ provides an upper limit.

For sediment transport, we use the Meyer-Peter Mueller relation (MPM) (Meyer-Peter and Mueller, 1948):

$$q_s = 8\sqrt{Rgd^3}\,(\tau_* - \tau_{*c})^{3/2} \tag{8}$$

The appearance of g in this equation scales the model to Martian gravity. Substituting Eqs. (4)-(8) into Eq. (3):

$$\frac{dJ}{dt} = \frac{4}{\pi D^2}\left(Q_{in} - \frac{8w_c H^{5/3}\sqrt{gS}}{d^{1/6}}\right) + \left(\frac{w_c}{w_v}\right)\frac{8\sqrt{Rgd^3}\,(\tau_* - \tau_{*c})^{3/2}}{L} \tag{9}$$

Dimensionless Shield's stress τ_* in the channel is found using:

$$\tau_* = \frac{HS}{Rd} \tag{10}$$

where R is submerged specific gravity, a dimensionless measure of sediment buoyancy in water ($R = \frac{\rho_{sediment} - \rho_{fluid}}{\rho_{fluid}}$). The ratio of Shields stress τ_* to critical Shields stress τ_{*c} can be expressed in

terms of the transport stage (T), where $T < 1$ indicates no bedload sediment transport:

$$T = \frac{\tau_*}{\tau_{*c}} \tag{11}$$

To solve Eq. (9) we discretize Eq (9) such that:

$$J_{i+1} = J_i + \Delta t \left[\frac{4}{\pi D^2} \left(Q_{in} - \frac{8 w_c \left(\frac{2}{3} J_i\right)^{5/3} \sqrt{gS}}{d^{1/6}} \right) + \left(\frac{w_c}{w_v}\right) \frac{8\sqrt{Rgd^3} \left(\left(\frac{2 J_i S}{3Rd}\right) - \tau_{*c} \right)^{3/2}}{L} \right] \tag{12}$$

where the subscript i indicates the ith timestep. We numerically integrate Eq. (12) from $t = 0$ to $t = 1$ year with $\Delta t = 100$ s.

In the first part of our analysis, we assume $Q_{in} = 0$, i.e. no flow into the crater during overspill. Under these conditions, our model predicts 2 possible regimes for breach erosion:

1. *Runaway erosion*
   Favored by large lakes with narrow, steep channels and short valleys (large D and S, small w_v and L). At the onset of erosion, the outlet channel erodes downwards faster than q_{out} reduces lake level. Eq. (3) is positive. Water depth H in the channel increases. This increases erosion rate in the channel (Eqs. (8) & (10)), but q_{out} increases more rapidly (Eq. (6)). H increases until the rate of lake level change dE/dt matches channel floor erosion rate dB/dt (i.e. Eq. (3) goes to zero). Erosion continues at a constant rate until the lake is drained, i.e. all available topography is consumed, corresponding to erosion of the valley floor through the entire elevated crater rim.
2. *Self-arrest erosion*
   Favored by small lakes with wide, gently-sloping channels and long outlet valleys (small D and S, large w_v and L). At the onset of erosion, q_{out} reduces lake level faster than the valley floor erodes. Eq. (3) is negative. Water depth in the channel decreases. This reduces sediment transport rate in the channel more rapidly than it reduces q_{out} of the channel (Eqs. (8) & (10) vs. (6)), so Eq. (3) remains negative. Once H drops below the sediment transport threshold, erosion stops and $dB/dt = 0$. q_{out} asymptotes to 0 before the lake is drained, i.e. not all available topography is consumed.

When there is flow into the lake ($Q_{in} > 0$), a third, sustained erosion regime occurs (discussed in Section 5), where the channel is able to accommodate q_{out}, but Q_{in} exceeds the sediment transport threshold. This causes continuous erosion in the channel at a fixed rate.

Exit breach channel and eroded valley widths are indistinguishable in most pollywog DEMs. We assume that the channel width does not change during the overspill event, and that the channel occupied the full valley width, i.e. $w_c = w_v$ and $\frac{w_c}{w_v} = 1$. This represents a rectangular, trough-shaped channel. If initial channel widths were much narrower than the observed valley width, or $w_c < w_v$, runaway is more likely because less water will drain from the lake at each timestep. This keeps water depth and erosion rates in the channel high (Eq. (10)). In the natural case we would expect channel width to vary with time as H evolves. In the event of self-arrest erosion, H decreases over time so we expect channel widening to occur early in the overspill event. $w_v \approx w_c$ is also likely a good approximation for pollywogs based on analogue experiments of crater breaches (Marra et al., 2014), which suggest channel width and valley width are similar during crater rim breach floods.

The most important uncertainties in our model are initial flow depth and grainsize. These parameters set initial Shields stress τ_* (Eq. (10)), which determines the initial rate of channel incision (Eq. (8)). When $\tau_* > \tau_{*c}$, sediment transport can occur. $\frac{dB}{dt}$ decays rapidly during self-arrest erosion (Fig. 5). Higher initial transport stages lead to more rapid initial erosion and allow erosion to occur for longer. The measured breach channel depth for the pollywog in Fig. 1b is 17.6 ± 1.8 m. We assume initial flow depth must be much smaller and use initial breach depths of 1 and 10 m, where 10 m is approximately 10% of the deepest measured pollywog breach. We use a shear stress parameterization and τ_{*c} appropriate for gravel-sized grains. The only constraint on grainsize is that individual clasts cannot be seen at a 25 cm pixel^{-1} resolution in HiRISE images. Observations of impact breccia from Victoria Crater suggest most clasts are <1 m in diameter (Squyres et al. (2009), Fig. 3). To avoid assuming a grainsize, we find the optimal grainsize for erosion (i.e. the grainsize for which maximum erosion occurs) for each pollywog numerically. As a result, we likely overestimate erosion. Application of the Meyer-Peter Mueller relation (Eq. (8)) is discussed in Section 4.1.

3. Results

We apply our model to Mars pollywogs (Section 3.1) and terrestrial breach erosion events compiled from the literature (Section 3.2).

3.1. Mars pollywogs: measurements & implications

We constructed DEMs for 18 craters with exit breaches (Table 1) using PDS-released HiRISE stereopairs and tools developed by Mayer and Kite (2016) (streamlined by S. Holo). We used these DEMs to measure pollywog crater exit breaches (Table 2). We mark pollywogs as consistent with runaway erosion if our model predicts runaway for all combinations of measured parameters (D, S, L, w_v) (Fig. 4). In our fixed channel width 0-D model, runaway is independent of grainsize because whether the lake can drain fast enough to cause water depth in the channel to drop is controlled by channel geometry and lake size (Eq. (4)). We find the runaway threshold numerically for each pollywog by varying S for $H_0 = 1$ m. Our model predicts runaway erosion for two pollywogs (breaches 4 and 13a, Table 1 and Fig. 4). The measured fraction of eroded relief for these pollywogs is <0.65, so the channels did not erode through their crater rims. This model–data disagreement is discussed in Section 4.

We used valley geometry measurements as inputs to our breach erosion model and calculated eroded breach depth for initial flow depths $1 < H_0 < 10$ m and grainsizes $0.01 < d < 1$ m. A pollywog is consistent with a single erosion event if model-predicted total eroded depth meets or exceeds measured breach depth z_v for any grainsize d. To quantify the single to multiple event threshold, we found the critical value of $w_v/S^{7/6}$ required for each pollywog to erode in a single event for 3 logarithmically-spaced initial flow depths (10^0, $10^0.5$, and 10^1 m). We assumed a log-uniform prior for initial flow depth and a linear relationship between $w_v/S^{7/6}$ and D^2/L to perform 15,000 bootstraps to find the 95% confidence interval for a pollywog breach eroding in a single, self-arrest overflow event (Fig. 4). Assuming $Q_{in} = 0$, three pollywogs fall outside this region of parameter space. These three pollywogs require multiple events to erode the observed breaches, or $Q_{in} \neq 0$. We discuss this in Section 5.

3.2. Application of the model to terrestrial breaching events

We tested our model against some potential pollywog terrestrial analogues, including outburst floods from moraine-dammed

Table 2
Measured pollywog exit breach parameters from DEMs. L is outlet valley length. w_v is valley width, measured as the distance between the upper breaks in slope of the valley walls in cross sections of the exit breach. z_v is breach depth relative to the adjacent crater rim, measured using cross sections of the exit breach. $S_{channel}$ is the maximum valley bed slope, measured using long profiles down the center of the exit breach valley. S_{rim} is the average crater rim slope measured either side of the exit breach valley. Error estimates are standard deviations of 4 measurements. V is the volume of the crater. Breach numbers map to Table 1.

Breach		L (km)	w_v (m)	z_v (m)	$S_{channel}$	S_{rim}	V (km^3)
1		5.8 ± 0.4	549 ± 48	41 ± 12.2	0.03 ± 0.01	0.17 ± 0.07	135.61 ± 3.06
2		1.4 ± 0.0	100 ± 8	5 ± 0.8	0.10 ± 0.01	0.10 ± 0.03	0.47 ± 0.03
3		2.5 ± 0.1	35 ± 15	1 ± 0.8	0.09 ± 0.02	0.15 ± 0.02	0.07 ± 0.00
4		4.4 ± 0.1	208 ± 12	44 ± 4.3	0.09 ± 0.02	0.10 ± 0.00	38.07 ± 1.32
5		20.7 ± 0.1	474 ± 34	71 ± 4.9	0.13 ± 0.02	0.29 ± 0.02	213.34 ± 4.65
6		8.5 ± 0.5	878 ± 42	116 ± 15.1	0.12 ± 0.06	0.17 ± 0.05	56.74 ± 11.06
7		1.5 ± 0.0	297 ± 17	35 ± 1.9	0.07 ± 0.03	0.11 ± 0.05	19.37 ± 2.13
8		1.4 ± 0.0	254 ± 56	40 ± 3.7	0.07 ± 0.01	0.09 ± 0.01	8.45 ± 0.34
9		2.0 ± 0.2	247 ± 23	34 ± 2.0	0.14 ± 0.03	0.09 ± 0.03	4.78 ± 0.75
10		4.5 ± 0.1	300 ± 44	25 ± 1.7	0.11 ± 0.01	0.14 ± 0.04	3.05 ± 0.06
11		10.7 ± 0.2	453 ± 85	46 ± 2.7	0.06 ± 0.02	0.09 ± 0.03	141.50 ± 16.01
12		3.1 ± 0.1	265 ± 37	18 ± 1.8	0.07 ± 0.01	0.08 ± 0.02	5.03 ± 0.23
13	a	3.7 ± 0.1	257 ± 23	31 ± 0.7	0.15 ± 0.03	0.22 ± 0.06	16.50 ± 1.17
	b	5.4 ± 0.2	308 ± 35	46 ± 4.6	0.08 ± 0.02	0.16 ± 0.01	
	c	3.7 ± 0.2	249 ± 21	28 ± 2.8	0.10 ± 0.01	0.13 ± 0.07	
14	a	3.3 ± 0.1	227 ± 52	20 ± 4.2	0.10 ± 0.01	0.19 ± 0.04	10.11 ± 1.96
	b	1.8 ± 0.1	197 ± 12	19 ± 3.6	0.11 ± 0.01	0.21 ± 0.03	
15		0.8 ± 0.0	228 ± 35	28 ± 1.4	0.15 ± 0.01	0.16 ± 0.03	0.62 ± 0.05
16		3.9 ± 0.1	265 ± 13	31 ± 4.2	0.08 ± 0.03	0.09 ± 0.03	22.09 ± 3.28
17		0.3 ± 0.0	145 ± 3	16 ± 2.0	0.14 ± 0.04	0.14 ± 0.03	0.01 ± 0.00
18		1.4 ± 0.1	200 ± 27	21 ± 1.0	0.07 ± 0.00	0.16 ± 0.05	0.12 ± 0.01

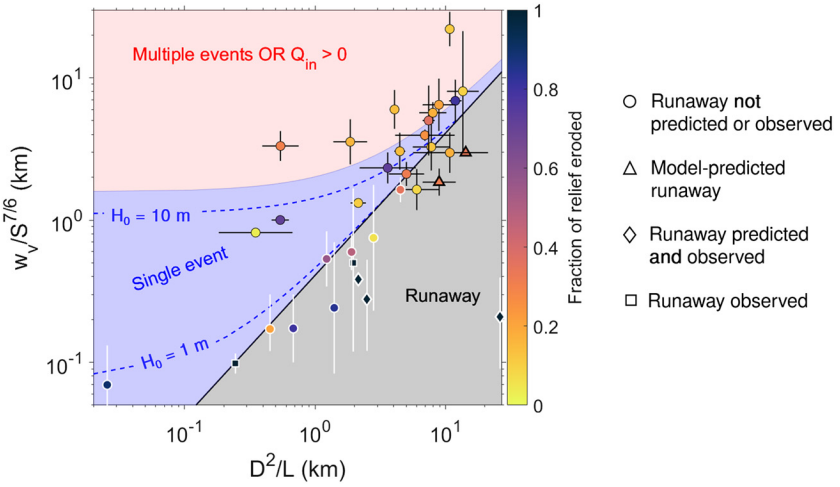

Fig. 4. Lake size relative to outlet valley length plotted against valley width and steepness for pollywogs and terrestrial analogues. Thresholds for runaway erosion and multiple erosion events/erosion events with continued water supply to the crater are found numerically by comparing model predicted erosion depth to measured pollywog outlet breach depths. Black outlines/bars are Mars pollywog data (Table 2). Bars show the range between maximum and minimum measured values (individual measurement errors are negligible by comparison). Markers are at the logarithmic mean of maximum and minimum values. White outlines/bars are Earth dam breach events. Markers are plotted at the mean measured value if available, or at the logarithmic mean of the measured range. Black line indicates the runaway threshold. Triangular markers: runaway is always predicted by the model. Square markers: runaway erosion is observed (i.e. all available relief consumed). Diamond markers: runaway is predicted by the model and measured in reality. Blue shaded area: 95% confidence interval from 15,000 bootstraps for transition between an eroded breach being consistent with a single overspill event to requiring multiple events for initial flow depths $1 < H_0 < 10$ m assuming a log-uniform prior for H_0. 3 Mars pollywogs require multiple erosion events or continuous input of water into the crater to erode the observed outlet breach depth. Our model predicts runaway erosion for 2 pollywogs.

lakes, landslide dams, and caldera lakes (Fig. 4). Our model results are sensitive to breach length and channel slope, so we selected historical events with well-documented pre- and post-breach topography to test the model. Where breach valleys connect to pre-existing channels, we used pre-breach dam width (where available) as a lower bound on eroded channel length. Otherwise, we assume a conservative (i.e. short) channel length $L = D/2$. This favors runaway. Most well-documented moraine/landslide dammed lake breaches erode all available relief. Our model predicts runaway erosion under all conditions for 3 out of 5 known to be runaway events based on relief consumed during flooding (Fig. 4). The remaining two events are consistent with runaway in the model within the range of measured slopes and channel widths. This slight underprediction of terrestrial runaway erosion reinforces our conclusion that two of the measured pollywog craters would be expected to undergo runaway breach erosion during crater overspill.

Using moraine/landslide dams and volcanic caldera lake breaching events to test our model has several limitations. Firstly, our model assumes that abundant, loose sediment is available in the channel (transport-limited erosion). This might not apply to volcanic calderas where the caldera walls are formed primarily of

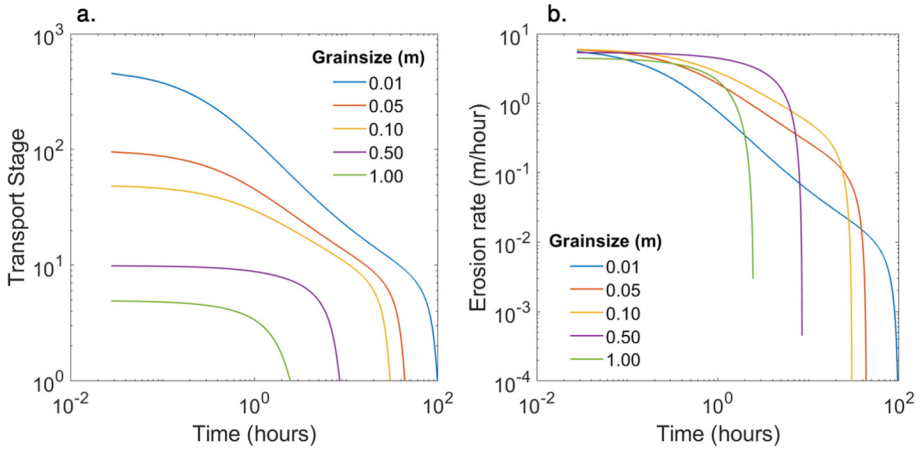

Fig. 5. Model-predicted evolution of a. transport stage T (the ratio between Shields stress τ_* and the critical Shields stress for sediment transport τ_{*c}) and b. erosion rate over time since breach initiation for the Pinatubo Caldera breaching event in 2002 (Lagmay et al., 2007), assuming $H_0 = 1.54$ m and $Q_{in} = 0$. No erosion occurs when the transport stage falls below 1. The duration of the real event was <24 hours. This illustrates the general evolution of self-arrest erosion.

lava flows. Intact rock needs to be broken into clasts before sediment transport can occur (detachment-limited erosion). Secondly, our model assumes uniform grainsizes between 0.01 and 1 m. Moraine deposits, landslides, and caldera walls can have a wide range of grainsizes, and a large proportion of fines (Lagmay et al., 2007; Clague and Evans, 2000). Gravel-sized clasts may be a poor approximation to the real dam grainsize distribution. This also applies to impact ejecta. Thirdly, interstitial ice in some moraine dams (Clague and Evans, 2000) may change the erodibility of dam materials by freezing clasts together. Additionally, ice melting during breaching this would lower the channel floor faster than erosion alone. Finally, available terrestrial examples of lakes draining through erosion of an exit breach and outlet valley are much smaller than the majority of pollywog craters measured on Mars ($\bar{D}_{terrestrial} = 1.44$ km, $\bar{D}_{Mars} = 5.26$ km). These differences in size may mean that different lake draining behaviors should be expected.

4. Runaway erosion: predicted but not observed

Runaway erosion is observed for many terrestrial moraine/landslide dam breaching events (i.e. erosion to the base of the dam), whether the dam is a landslide deposit, terminal moraine, or crater rim. Runaway erosion is not observed for any pollywog valleys. Pollywog exit breaches do not erode deeply relative to crater floor depth (Fig. 1). By contrast, megaflood-formed valleys in Xanthe Terra erode hundreds of meters of crust (Coleman, 2005), representing 80 to 100% of the available relief (e.g. Shalbatana Valles, Masursky Crater outflow valleys at 12.964°N, −32.497°E). The water supply mechanism for pollywogs cannot be both intense and long-lived. Our model predicts runaway erosion for at least two pollywog exit breaches. However, our model likely overestimates erosion. Firstly, measured w_v is an upper limit on channel width. If active channel width, which cannot be measured directly, was smaller than valley width, this would favor runaway. Setting $w_c/w_v = 1/3$, the number of runaway breaches predicted by the model increases sixfold (to 13/22). Secondly, our baseline model assumes no water flux into the crater during erosion ($Q_{in} = 0$). This minimizes dH/dt, disfavoring runaway erosion. Therefore, if pollywog overspill occurs during a climate event with increased runoff, or during a groundwater outflow event, runaway will be more likely than captured by the model. Typical measured breach depths are <50% (mean = 0.4, median = 0.3) of the available relief. This lack of observed runaway erosion may provide additional information about whether pollywog breaches can form in a single event, and whether or not pollywogs were predominantly ice-filled. There are three possible explanations for the lack of observed runaway erosion:

- **Hypothesis 1:** – The Meyer-Peter Mueller equation (MPM) for capacity bedload transport overpredicts pollywog valley erosion (Section 4.1).
- **Hypothesis 2:** – The stratigraphic transition from crater rim ejecta to uplifted bedrock is sufficient to halt runaway erosion (Section 4.2).
- **Hypothesis 3:** – Channel length (L), channel slope (S), or crater diameter (D) measured from DEMs are not representative of crater overspill conditions (Section 4.3).

4.1. Sediment transport on steep slopes

The empirical MPM equation for bedload transport was determined for well-sorted, gravel-bedded, terrestrial rivers, with shallow slopes ($\ll$0.1) (Meyer-Peter and Mueller, 1948). Measured pollywog valley floor/crater rim slopes fall in the range $0.03 < S < 0.29$. There is some debate whether MPM under or overpredicts erosion in steep channels (Damgaard et al., 1997; Cheng and Chen, 2014). Increased τ_{*c} on steep slopes disfavors runaway (Eq. (9)). Flume experiments by (Lamb et al., 2008), and τ_{*c} measurements made in terrestrial gravel bedded streams/rivers (Mueller et al., 2005), suggest τ_{*c} reaches 0.1 at slopes $S > 0.02$. Even with $\tau_{*c} = 0.1$, our model predicts runaway for the two pollywogs identified in Fig. 4. Our results are not strongly sensitive to the value of τ_{*c}. Given uncertainty in the correction for τ_{*c}, agreement between our model and terrestrial observations, and the small effect of doubling τ_{*c}, we do not modify τ_{*c}.

The mean sediment:water ratio for pollywogs consistent with a single overspill event is 0.07 by volume. 0.04 is expected for water floods (Pierson, 2005). High sediment concentrations can lead to strongly non-Newtonian behaviors in sediment-water mixtures (Pierson, 2005). High sediment concentrations increase flow density, which may increase bedload transport. However, the primary effect of hyperconcentration on sediment transport is a decrease in suspended sediment settling rates. MPM performs well for hyperconcentrated flows up to high (∼20%) sediment concentrations on steep slopes in analogue and numerical experiments (Rickenmann, 1991; Abderrezzak and Paquier, 2011). We disfavor Hypothesis 1 to explain the lack of runaway, and do not adjust our sediment transport equation for hyperconcentration.

4.2. Barriers to crater rim erosion

Crater rims are composed of uplifted bedrock overlain by ejecta. The contact between crater ejecta and bedrock is visible in the fresh impact crater visited by the Mars Exploration Rover Opportunity (Victoria Crater) (Squyres et al., 2009). The transition from poorly consolidated ejecta to intact bedrock could inhibit runaway erosion by a change in the erosion mechanism, or a change in grainsize. Our model assumes breach erosion is limited by whether the shear stress at the base of the channel is strong enough to move loose sediment clasts (transport-limited erosion). In bedrock, erosion is limited by whether the shear stress is sufficient to break off new clasts from the intact rock (detachment-limited erosion; Whipple et al. (2013)). Moving pre-existing clasts requires lower Shields stress than breaking off new clasts. Recent bedrock river studies suggest that plucking is one of the primary mechanisms of bedrock erosion (Lamb et al., 2015; Whipple et al., 2013). Plucking occurs when water breaks up bedrock along joint planes (Lamb et al., 2015). Larsen and Lamb (2016) apply a plucking threshold (τ^*_{pc}) to bedrock erosion in the Channeled Scablands:

$$\tau^*_{pc} = \frac{\cos\theta\,[\tan\phi - \tan\theta] + 2\tau^*_w}{\left[1 + \frac{1}{2}C_D\left(\frac{u}{u_*}\right)^2 \frac{p}{L}\right]\left[1 + F^*_L \tan\phi\right]} \quad (13)$$

where θ is bed angle in degrees ($S_{channel} < \theta < S_{rim}$), ϕ is bed friction angle (wet basalt), τ^*_w is dimensionless block sidewall stress (caused by friction along the sides of a block of fractured bedrock), C_D is a local drag coefficient for fractured bedrock blocks related to particle Reynolds number (Lamb et al., 2015), $\frac{p}{L}$ is the ratio of protrusion height of basalt blocks above the channel floor to the length of each block, $\frac{u}{u_*}$ is the ratio of flow velocity to bed shear velocity, and F^*_L is the dimensionless hydraulic lift (force exerted perpendicular to the channel bed by flow of water over bedrock). We adopt the same values for these parameters as (Lamb et al., 2015) to find an upper limit on τ^*_{pc}, setting $\cos\theta \approx 1$, $\tan\theta \approx 0$ (i.e. a very gently sloping channel), and letting $\frac{p}{L}$ approach 0 (i.e. blocks protrude very little above the bed). This gives $\tau^*_{pc} \approx 0.65$, equivalent to $T \approx 13$. $T > 13$ is readily achieved in all pollywog exit breach valleys at the beginning of a breach event, assuming optimal grainsize for erosion (Section 5). During runaway erosion, T increases over time as the lake drains through a breach that is not large enough to accommodate $q_{w,out}$. A transition from transport-limited to detachment-limited, plucking-dominated erosion would be insufficient to inhibit runaway. If the ejecta-bedrock transition inhibits runaway through a change from transport-limited to detachment-limited erosion, we would expect to see only multiple erosion event pollywog breaches incising into bedrock.

A change in grainsize at the ejecta-bedrock boundary could also inhibit runaway erosion. Large grainsizes (approaching 1 m) erode less efficiently in the model (Fig. 5) because $T \propto \frac{1}{d}$. During runaway erosion, T initially increases rapidly, then plateaus at a maximum value. If this maximum transport stage is less than the maximum ratio of $\frac{d_{bedrock}}{d_{ejecta}}$ (the range of grainsizes in the model gives $\left(\frac{d_{bedrock}}{d_{ejecta}}\right)_{max} = 100$), then a change in grainsize could halt runaway erosion, because T would fall below 1 when the grainsize change occurs (assuming an instantaneous ejecta to bedrock transition), this corresponds to cessation of erosion. However, this is not the case for either pollywog for which our model predicts runaway (Table 1). For breach 4 ($T_{max} \approx 2800$), and for breach 13 ($T_{max} \approx 600$). However, we select a grainsize to maximize erosion, so T_{max} during crater overspill was likely less than predicted. If the ejecta-bedrock transition inhibits runaway through an abrupt, order of magnitude change in grainsize, we would not expect to see pollywog exit breach valleys incise into bedrock. To test this prediction, we can compare breach depths to predicted ejecta thickness (Fig. 6). There are only a handful ejecta thickness observations for Martian craters (Sturm et al., 2016), and the contact between ejecta and bedrock is not visible in the pollywog HiRISE images. From existing data, there is no clear relationship between fraction of eroded relief and number of overspill events required (Fig. 4). The uncertainty in the ejecta thickness/crater diameter relationship means that the ejecta-bedrock transition – Hypothesis 2 – cannot be ruled out as a mechanism for halting breach erosion.

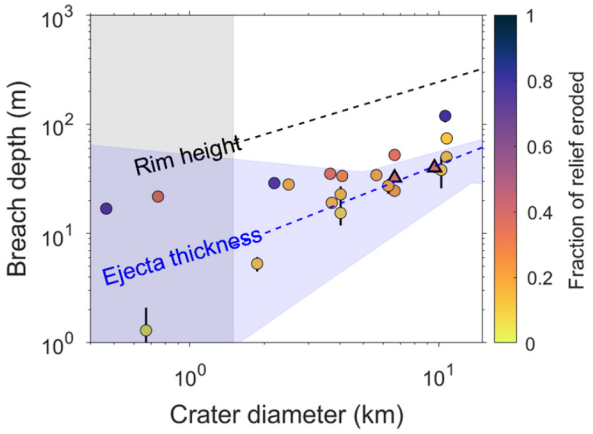

Fig. 6. Measured pollywog exit breach depth vs. crater diameter. Marker color indicates fraction of available relief eroded by the breach. Dashed black line shows an empirically derived relationship between crater diameter and rim height for pristine craters (Mouginis-Mark et al., 2018). Dashed blue line shows a powerlaw fit to ejecta thickness and crater diameter measurements in Sturm et al. (2016). Grey shaded area indicates diameter range not covered by rim height and ejecta thickness relationships. Blue shaded area shows a bootstrapped 95% confidence interval on Sturm et al. (2016) based on crater measurements ($n = 5000$).

4.3. Pre-event vs. measured breach morphology

Pollywog measurements from DEMs may not be representative of crater and channel morphology during overspill. We assume $w_c = w_v$, likely overestimating active channel width during erosion. This disfavors runaway. There are three remaining parameters that could explain the lack of runaway erosion if their present day values are not representative of the breaching event.

1. *Slope (S)*
   If channel slope during overspill was less than DEM measured $S_{channel}$ runaway would be less likely. For a crater overspilling for the first time, the initial channel slope would be the slope of the crater rim. S_{rim} is typically steeper than $S_{channel}$, therefore shallower initial breach channels are unlikely, favoring runaway. Slope cannot explain the data-model discrepancy.
2. *Channel Length (L)*
   Increasing channel length L decreases likelihood of runaway because erosion occurs over a larger area. This decreases the magnitude of dB/dt, making lake draining more likely to outpace downward erosion in the channel (Eq. (3)). This favors self-arrest erosion (Section 2.1). For most pollywogs, $L = (0.8 \pm 0.8)D$. Pollywogs are identified, in part, by the fresh appearance of their crater rims, precluding extensive erosion (Wilson et al., 2016) as an explanation for the short exit breach valleys observed. The two pollywogs for which runaway is predicted do not connect to a larger drainage network, so a difference in L is unlikely to explain the lack of runaway.
3. *Lake Diameter: Water-filled vs. Ice-filled craters*
   Measured crater diameter D may overestimate the size of the lake that drained to form the pollywog exit breach. Some pol-

lywogs have debris-covered icy deposits on their crater floors. If the crater was predominantly ice-filled during overspill, formation of a melt pond could form a lake with a much smaller equivalent diameter than the crater. Ice could also act as a barrier to crater rim erosion. If pollywogs were predominantly ice filled (discussed in Section 5.1) with a meltwater lake, runaway could be prevented simply by the meltwater lake volume being too small to supply water to erode through the crater rim. This is an attractive mechanism for pollywog formation because it does not require the full crater volume to be filled with liquid water.

5. Are all pollywogs consistent with a single overspill event?

The transition between breaches consistent with a single overspill event and breaches that require multiple breaching events or continuous supply of water (termed "multiple event" breaches) depends on how fast the lake can drain relative to the size of the lake. This can be quantified using the $w_v/S^{7/6}$ ratio of an outlet valley, and D^2/L of the pollywog crater and outlet valley. The power of 7/6 is inherited from Eqs. (6) & (8). We define the transition as the value of $w_v/S^{7/6}$ that allows for the observed breach depth to be eroded in a single event. This critical $w_v/S^{7/6}$ ratio is found numerically. At large D^2/L, the single-multiple event transition is close to the runaway threshold. Based on our modeling results, three pollywog exit breach valleys cannot be eroded through a single breaching event (Fig. 4). These pollywogs require water flux into the crater during overspill, or multiple overspill events. The required water flux into the crater, flux duration, and the implied annual average flux can be compared to previously published estimates of potential pollywog water sources, such as groundwater, rainfall, and snowmelt runoff.

Water flux into the lake (Q_{in}) must be large enough that $\tau_* > \tau_{*c}$ (Eqs. (10) & (8)) for erosion to continue. To ensure we only reject a hypothesis if absolutely necessary, we total required water volume by assuming the most favorable grainsize for erosion for each pollywog. This maximizes eroded depth during the self-arrest portion of erosion (i.e. the initial breach). We solve for critical $Q_{in,crit}$ using a bisection method. When $Q_{in} = Q_{in,crit}$, the breach will take an infinite amount of time to erode. We ran our model with $Q_{in} = XQ_{in,crit}$, where X is a multiplier from 1.1 to 100, and found the time t_z at which total modeled eroded depth was equal to measured breach depth (Fig. 7). We found flux of water per unit lake area q_w using:

$$q_w = \frac{4Q_{in}}{\pi D^2} \tag{14}$$

q_w and t_z were used to calculate the implied annual average water supply rate. This can be compared to predictions for annual average precipitation/snowmelt under various climate scenarios (Kite et al., 2019; Turbet et al., 2020) (Section 5.1), and estimates of groundwater discharge (Section 5.2). None of the three pollywog crater exit breaches are consistent with formation in a single event with water input to the crater from energy limited snowmelt (4 m yr^{-1}). They are only consistent with a single event if there is groundwater discharge into the crater.

In future work, we aim to determine whether pollywog craters with multiple, deep exit breach valleys (e.g. craters 13 & 14 in Table 1) are consistent with formation during a single event. In single outlet pollywogs, the exit breach is always on the crater rim's lowest point. If a crater overspilled multiple times, we would expect water to flow through the pre-existing valley. The terrestrial pollywog overspill analogues in this study (Section 3.2) only have one outlet valley. Possible explanations for multiple outlet valleys include blockages of a pre-existing exit breach by ice (as there are

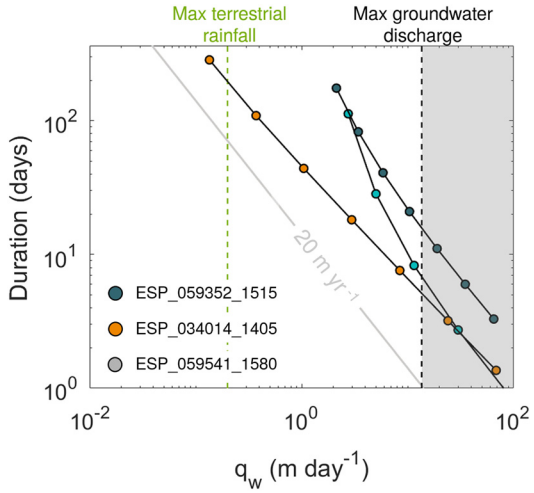

Fig. 7. Water flux into the crater q_w per unit lake area and required duration to erode observed breach depth. Grey contour shows an annual average water flux per unit lake area of 20 m yr^{-1}. 4 m yr^{-1} is the maximum for energy limited snowmelt (Kite et al., 2019). Green dashed line shows maximum daily precipitation rate for extreme terrestrial rainfall events (Chien and Kuo, 2011). This precipitation rate is only sustained for hours to days, not a full year. Dashed black line shows the maximum possible discharge from a 1 km deep ice-pressurized aquifer (Section 5).

no blockages visible at present in DEMs), regional tilting between overspill events due to lithospheric loading (ice sheets, volcanic edifices), and formation of multiple, spatially isolated melt ponds on the surface of a crater-filling ice body (similar to Fig. 2b). Understanding how multiple valleys can drain the same crater may be critical to understanding whether or not pollywogs were predominantly ice filled, and whether multiple-exit breach craters can ever be formed in a single overspill event.

5.1. Climate pollywog overspill scenarios

If pollywog overspills are climate-induced, then climate during their formation must have supplied large volumes of water as rain or snowfall. Large impacts are frequently proposed for inducing short term increased precipitation rates on Mars. Mars General Circulation Models (GCMs) seeded with impact model outputs produce precipitation rates up to 3 m yr^{-1} (Steakley et al., 2019; Turbet et al., 2020). For impacts producing craters ~600 km, this precipitation can last decades (Steakley et al., 2019; Turbet et al., 2020). There are several problems with an impact trigger for pollywog overspill. Firstly, the 6 largest Hesperian and Amazonian impact craters have diameters <250 km (Irwin, 2013). Secondly, the impact generated precipitation would mostly fall as snow rather than rainfall (Steakley et al., 2019), so the maximum volume of surface liquid water would still depend on energy-limited, melt-derived runoff. The total integrated precipitation following a large bolide impact is modest even for bolides forming ~ 600 km diameter craters entering a 1 bar Mars atmosphere; with a maximum of 10 m (Steakley et al., 2019) to 50 m (Turbet et al., 2020). This would only be sufficient to overspill the five smallest pollywogs in this study, which all have rim to floor depths of <50 m. Precipitation from a large impact would be insufficient to sustain erosion in an exit breach channel. Even if impact induced precipitation is much more intense than predicted by models, the most extreme rainfall rates recorded on Earth (Chien and Kuo, 2011) would also not be able to provide the required q_w. Additionally, impact induced precipitation is not globally uniform (Turbet et al., 2020; Steakley et al., 2019). Steakley et al. (2019) show that precipitation following a large impact is concentrated in the Northern midlatitudes, regardless of impact location, which may be consistent with the high density of pollywogs observed in Arabia

Terra (Wilson et al., 2016), but not the global pollywog distribution. However, a bolide impact could increase Mars' surface temperature even in a 150 mbar atmosphere (Steakley et al., 2019), which could contribute to snowmelt runoff.

Without extreme, isolated changes in climate generating large volumes of precipitation or melting, orbitally-driven climate oscillations are a more plausible explanation if pollywog overspill is primarily climate-driven. The most important climate constraint provided by pollywogs is that a crater must first be filled in order to overspill. This requires accumulation of large volumes of ice or liquid water. This is consistent with observations of ice-related features in the Martian midlatitudes (Fassett et al., 2010), and models of ice accumulation under different orbital conditions (Mischna et al., 2013). Ice-related formation mechanisms have also been proposed for features associated with pollywog occurrence in Arabia Terra such as fresh shallow valleys (Wilson et al., 2016).

Ice accumulation in mid latitudes during the Hesperian could gradually fill pollywog craters. Once ice-filled, seasonally or orbitally driven meltwater production (i.e. an excursion to temperatures above freezing) would enable some exit breach erosion through draining of a meltwater lake on the ice surface. This hypothesis is consistent with erosion of <60% of the available relief by 80% of pollywog exit breach valleys because a meltwater lake would have a smaller volume of water available for erosion. If pollywog overspill was caused by warming and increased melt production, the effects would not be localized to regions with pollywogs, but would leave a global signature. Low latitude alluvial fan activity is evidence for surface liquid water during the Hesperian and Amazonian (Hauber et al., 2013). However, the preferential occurrence of pollywogs in midlatitudes (Wilson et al., 2016) indicates that these potentially contemporaneous alluvial fan forming wet events were insufficient to lead to overspill of low latitude craters. Latitudinal differences in ice availability (e.g. snowpack vs. crater-filling ice pods) would make equatorial craters less likely to overspill, while still making meltwater available for alluvial fan deposition.

In this scenario, however, it is more difficult for all exit breach erosion to occur during a single overspill event for any of the pollywogs because the water depth must extend to at least the base of the channel. To melt ice filling a pollywog to the measured breach depth across the entire crater area would exceed the energy limited snowmelt rate of 4 $\mathrm{m\,yr^{-1}}$ (Kite et al., 2013) for all but one pollywog (Table 1 & 2, breach 3). Therefore, either a shallower meltwater lake would form or the diameter of the meltwater lake would be smaller, reducing the eroded depth in a single event. This favors multiple events for pollywog breach erosion if pollywog overspill was climate driven, and is consistent with the lack of observed runaway erosion.

5.2. Groundwater pollywog overspill scenarios

Previous work on Mars hydrology and groundwater outburst floods (e.g. Hanna and Phillips (2005)) sets an upper limit on groundwater discharge from a pressurized aquifer. Assuming that the conduit between the aquifer and the crater floor is already water saturated, we can use Darcy's law:

$$q_{max} = \frac{K \Delta P_{max}}{\mu z_{min}} \tag{15}$$

where K is aquifer permeability, and $\mu = 8.9 \times 10^{-4}$ Pa s is the dynamic viscosity of water. The maximum pressure P_{max} within a Martian aquifer is set by the tensile strength of the bedrock. For Mars, we assume a basaltic crust with tensile strength 2-14 MPa (Schultz, 1993). From existing estimates for Hesperian surface temperatures and heat flux, Harrison and Grimm (2005) predict a cryosphere thickness of several kilometers. The cryosphere must be >1 km thick to achieve superlithostatic pressures, but more likely >3 km (Wang et al., 2006). This is a lower limit on aquifer depth z_{min}. Assuming the fractured basalt megaregolith model of (Hanna and Phillips, 2005), Mars' crust has a permeability of order $K = 10^{-11}$ $\mathrm{m^2}$. For an aquifer depth of 1 km, and a tensile strength of 14 MPa, $q_{max} \approx 10$ $\mathrm{m\,day^{-1}}$ per unit crater floor area. More realistically, the flow of water would be focused through high permeability fractures ($\sim 10^{-9}$ $\mathrm{m^2}$ Wang et al. (2006)) with small cross sectional areas.

A groundwater trigger for pollywog overspill has several potential problems. Superlithostatic pressures are most easily achieved in a global aquifer (Hanna and Phillips, 2005), however, high aquifer pressures would enable high discharge rates to persist for days to months (Wang et al., 2006). This is inconsistent with the observation that no pollywog exit breaches have eroded through all the available topography, as would be expected for prolonged $Q_{in} > 0$. In a regionally dissected hydrological system with small, local aquifers, superlithostatic pressures may not be possible due to pressure diffusion out of the aquifer (Hanna and Phillips, 2005), so aquifer discharge would quickly decay (Wang et al., 2006), limiting the ability of the aquifer to both fill the pollywog and sustain $Q_{in} > 0$. Specific regional aquifer conditions would be required for a groundwater source to be consistent with pollywog breach depth observations. Finally, many pollywogs occur on regional or local highs (e.g. Fig. 1b), which is inconsistent with a groundwater source.

The size, latitude, and altitude distributions of pollywogs can also be used to constrain pollywog climate conditions and hydrology. Firstly, all known pollywogs are small (D <15 km). This apparent size cut-off has two possible explanations. Either water accumulation was insufficient to overspill craters D >15 km, or there was a lack of larger craters. From the pollywogs identified by Wilson et al. (2016) and the (Robbins and Hynek, 2012) crater database, 3% of craters in Arabia Terra with $D < 15$ km are pollywogs, i.e. the probability of any crater not being a pollywog is 0.97. There are 87 craters $D > 15$ km in the region studied by (Wilson et al., 2016). The probability of not finding a pollywog $D > 15$ km is 0.97^{87}, or 7%. While this suggests that there may be an upper limit on pollywog size, repeating this calculation with a global pollywog inventory is necessary. Secondly, ice accumulation is more strongly affected by latitude and altitude than groundwater. In the case of a global pressurized aquifer, the control on pollywog distribution would be the occurrence of conduits between the surface and the crater floor, which may not have any latitude/altitude preference at all. Conversely, ice accumulation is strongly sensitive to surface temperature and moisture distribution (Mischna et al., 2013).

6. Conclusions

Pollywogs are relatively young Martian craters with outlet valleys puncturing fresh crater rims, but no visible inlet valleys. Our new fixed channel width, 0-D model of breach erosion predicts runaway erosion for 2 of 21 measured pollywog crater exit breaches, but evidence for runaway erosion (defined here as erosion through the entire crater rim thickness) is not observed for any pollywogs. The mismatch between our model predictions and the measured pollywog valleys cannot be explained by increased critical dimensionless Shields stress (τ_{*c}) typical of steep slopes, different sediment transport equations, or differences in channel slope or outflow valley length. The remaining hypotheses are that runaway erosion is halted by the transition between impact ejecta and fractured, uplifted bedrock in the crater rim (either by a change in grainsize or a change in erosion style), or that the crater was predominantly ice-filled. There are two main scenarios for the

observed eroded depths of pollywog outlet valleys that are consistent with our modeling results:

1. Lots of erosion, once: Groundwater discharge infilled the crater with liquid water until it overspilled the rim, eroding the full valley depth in a single overspill event.
2. A little erosion, many times: Pollywog craters were predominantly filled with ice that underwent a small amount of melting many times (e.g. seasonally). This formed small melt ponds that drained over the crater rim, contributing a small amount of valley floor erosion each time the climate enabled meltwater to form.

While it is possible to fill and overspill a pollywog through a single groundwater discharge event, many pollywogs are located on local or regional highs which may argue against groundwater as a filling mechanism. No existing climate models for Hesperian Mars or impact-induced climates are capable of providing the precipitation rates or snowmelt rates required to fill and overspill a pollywog crater in a single event, which likely rules out the possibility of a single climate-induced pollywog-forming erosion event.

CRediT authorship contribution statement

A.O. Warren: Conceptualization, Data curation, Formal analysis, Investigation, Methodology, Software, Visualization, Writing – original draft. **S. Holo:** Methodology, Resources, Software, Writing – review & editing. **E.S. Kite:** Conceptualization, Funding acquisition, Supervision, Writing – review & editing. **S.A. Wilson:** Resources, Writing – review & editing.

Declaration of competing interest

The authors declare that they have no known competing financial interests or personal relationships that could have appeared to influence the work reported in this paper.

Acknowledgements

We thank Caleb Fassett for pointing out low latitude pollywogs, and the HiWish program for targetting requested pollywogs. We would also like to thank Tim Goudge and an anonymous reviewer for their insightful comments and suggestions which helped clarify the manuscript. We thank Shavonne Morin at the University of Arizona for producing the DEM in Fig. 1. All stereopairs are publicly available on the HiRISE website. Our DEMs are publicly available at https://uchicago.box.com/v/pollywog-DEMs2020. We acknowledge the use of University of Chicago Research Computing Center resources.

Grants: NASA NNX16AG55G (E.S.K.), NASA 80NSSC19K1221 (S.A.W.), and NASA NNX15AM49G (E.S.K.).

Appendix A. Supplementary material

Supplementary material related to this article can be found online at https://doi.org/10.1016/j.epsl.2020.116671.

References

Abderrezzak, K.E.K., Paquier, A., 2011. Applicability of sediment transport capacity formulas to dam-break flows over movable beds. J. Hydraul. Eng. 137 (2), 209–221. https://doi.org/10.1061/(ASCE)HY.1943-7900.0000298.

Andrews-Hanna, J.C., Phillips, R.J., 2007. Hydrological modeling of outflow channels and chaos regions on Mars. J. Geophys. Res., Planets 112 (E8).

Brownlie, W.R., 1983. Flow depth in sand-bed channels. J. Hydraul. Eng. 109 (7), 959–990.

Cheng, N.-S., Chen, X., 2014. Slope correction for calculation of bedload sediment transport rates in steep channels. J. Hydraul. Eng. 140 (6), 04014018.

Chien, F.-C., Kuo, H.-C., 2011. On the extreme rainfall of Typhoon Morakot (2009). J. Geophys. Res., Atmos. 116 (D5).

Clague, J.J., Evans, S.G., 2000. A review of catastrophic drainage of moraine-dammed lakes in British Columbia. Quat. Sci. Rev. 19 (17–18), 1763–1783.

Coleman, N.M., 2005. Martian megaflood-triggered chaos formation, revealing groundwater depth, cryosphere thickness, and crustal heat flux. J. Geophys. Res., Planets 110 (E12).

Damgaard, J.S., Whitehouse, R.J., Soulsby, R.L., 1997. Bed-load sediment transport on steep longitudinal slopes. J. Hydraul. Eng. 123 (12), 1130–1138.

Fassett, C.I., Dickson, J.L., Head, J.W., Levy, J.S., Marchant, D.R., 2010. Supraglacial and proglacial valleys on Amazonian Mars. Icarus 208 (1), 86–100.

Fassett, C.I., Head, J.W., 2008. Valley network-fed, open-basin lakes on Mars: distribution and implications for Noachian surface and subsurface hydrology. Icarus 198 (1), 37–56.

French, R.H., 1985. Open-Channel Hydraulics. McGraw-Hill, Stuttgart, New York.

Goddard, K., Warner, N.H., Gupta, S., Kim, J.-R., 2014. Mechanisms and timescales of fluvial activity at Mojave and other young martian craters. J. Geophys. Res., Planets 119 (3), 604–634.

Golombek, M.P., Grant, J.A., Crumpler, L.S., Greeley, R., Arvidson, R.E., Bell, J.F., et al., 2006. Erosion rates at the Mars exploration rover landing sites and long-term climate change on Mars. J. Geophys. Res., Planets 111 (E12).

Goudge, T.A., Fassett, C.I., Mohrig, D., 2019. Incision of paleolake outlet canyons on Mars from overflow flooding. Geology 47 (1), 7–10.

Hanna, J.C., Phillips, R.J., 2005. Hydrological modeling of the Martian crust with application to the pressurization of aquifers. J. Geophys. Res., Planets 110 (E1).

Harrison, K.P., Grimm, R.E., 2005. Groundwater-controlled valley networks and the decline of surface runoff on early Mars. J. Geophys. Res., Planets 110 (E12).

Hartmann, W.K., 2005. Martian cratering 8: isochron refinement and the chronology of Mars. Icarus 174 (2), 294–320.

Hauber, E., Platz, T., Reiss, D., Le Deit, L., Kleinhans, M., Marra, W., Carbonneau, P., 2013. Asynchronous formation of hesperian and Amazonian-aged deltas on Mars and implications for climate. J. Geophys. Res., Planets 118 (7), 1529–1544.

Holo, S., Kite, E., 2019. Dynamics of Mars lake-overflow valley incision. In: Lunar and Planetary Science Conference, vol. 50 (Abstract number 2481).

Irwin, R.P., 2013. Testing links between impacts and fluvial erosion on post-Noachian Mars. In: 44th Lunar and Planetary Science Conference (Abstract #2958). Lunar and Planetary Institute, Houston. Retrieved from http://www.lpi.usra.edu/meetings/lpsc2013/pdf/2958.pdf.

Jakosky, B.M., Henderson, B.G., Mellon, M.T., 1995. Chaotic obliquity and the nature of the Martian climate. J. Geophys. Res., Planets 100 (E1), 1579–1584.

Kamphuis, J., 1974. Determination of sand roughness for fixed beds. J. Hydraul. Res. 12 (2), 193–203.

Kite, E.S., Halevy, I., Kahre, M.A., Wolff, M.J., Manga, M., 2013. Seasonal melting and the formation of sedimentary rocks on Mars, with predictions for the Gale Crater mound. Icarus 223 (1), 181–210.

Kite, E.S., Mayer, D.P., Wilson, S.A., Davis, J.M., Lucas, A.S., Stucky de Quay, G., 2019. Persistence of intense, climate-driven runoff late in Mars history. Sci. Adv. 5 (3), eaav7710. https://doi.org/10.1126/sciadv.aav7710.

Lagmay, A.M.F., Rodolfo, K.S., Siringan, F.P., Uy, H., Remotigue, C., Zamora, P., Ong, J., 2007. Geology and hazard implications of the Maraunot notch in the Pinatubo Caldera, Philippines. Bull. Volcanol. 69 (7), 797–809. https://doi.org/10.1007/s00445-006-0110-5.

Lamb, M.P., Dietrich, W.E., Venditti, J.G., 2008. Is the critical shields stress for incipient sediment motion dependent on channel-bed slope? J. Geophys. Res., Earth Surf. 113 (F2).

Lamb, M.P., Finnegan, N.J., Scheingross, J.S., Sklar, L.S., 2015. New insights into the mechanics of fluvial bedrock erosion through flume experiments and theory. Geomorphology 244, 33–55.

Larsen, I.J., Lamb, M.P., 2016. Progressive incision of the channeled scablands by outburst floods. Nature 538 (7624), 229–232.

Marra, W.A., Braat, L., Baar, A.W., Kleinhans, M.G., 2014. Valley formation by groundwater seepage, pressurized groundwater outbursts and crater-lake overflow in flume experiments with implications for Mars. Icarus 232, 97–117. https://doi.org/10.1016/j.icarus.2013.12.026.

Matsubara, Y., Howard, A.D., Gochenour, J.P., 2013. Hydrology of early Mars: valley network incision. J. Geophys. Res., Planets 118 (6), 1365–1387.

Mayer, D.P., Kite, E.S., 2016. An integrated workflow for producing digital terrain models of Mars from CTX and HiRISE stereo data using the NASA Ames stereo pipeline. In: Lunar and Planetary Science Conference, vol. 47, p. 1241.

Meyer-Peter, E., Mueller, R., 1948. Formulas for bed-load transport. In: IAHSR 2nd Meeting. Stockholm. Appendix 2.

Mischna, M.A., Baker, V., Milliken, R., Richardson, M., Lee, C., 2013. Effects of obliquity and water vapor/trace gas greenhouses in the Early Martian climate. J. Geophys. Res., Planets 118 (3), 560–576.

Morris, M., Hassan, M., Kortenhaus, A., Visser, P., 2009. Breaching processes: a state of the art review. FLOODsite Report T06-06-03.

Mouginis-Mark, P.J., Boyce, J., Sharpton, V.L., Garbeil, H., 2018. Determination of Mars crater geometric data: insights from high-resolution digital elevation models. Meteorit. Planet. Sci. 53 (4), 726–740.

Mueller, E.R., Pitlick, J., Nelson, J.M., 2005. Variation in the reference shields stress for bed load transport in gravel-bed streams and rivers. Water Resour. Res. 41 (4).

Pierson, T.C., 2005. Hyperconcentrated flow—transitional process between water flow and debris flow. In: Debris-Flow Hazards and Related Phenomena. Springer, pp. 159–202.

Rickenmann, D., 1991. Bed load transport and hyperconcentrated flow at steep slopes. In: Armanini, A., Di Silvio, G. (Eds.), Fluvial Hydraulics of Mountain Regions. Springer, Berlin, Heidelberg, pp. 429–441.

Robbins, S.J., Hynek, B.M., 2012. A new global database of Mars impact craters $\geq$ 1 km: 2. Global crater properties and regional variations of the simple-to-complex transition diameter. J. Geophys. Res., Planets 117 (E6).

Rodriguez, J.A.P., Kargel, J.S., Baker, V.R., Gulick, V.C., Berman, D.C., Fairén, A.G., et al., 2015. Martian outflow channels: how did their source aquifers form, and why did they drain so rapidly? Sci. Rep. 5, 13404.

Schultz, R.A., 1993. Brittle strength of basaltic rock masses with applications to Venus. J. Geophys. Res., Planets 98 (E6), 10883–10895.

Squyres, S.W., Knoll, A.H., Arvidson, R.E., Ashley, J.W., Bell, J., Calvin, W.M., et al., 2009. Exploration of Victoria crater by the Mars rover opportunity. Science 324 (5930), 1058–1061.

Steakley, K., Murphy, J., Kahre, M., Haberle, R., Kling, A., 2019. Testing the impact heating hypothesis for early Mars with a 3-D global climate model. Icarus 330, 169–188.

Sturm, S., Kenkmann, T., Hergarten, S., 2016. Ejecta thickness and structural rim uplift measurements of Martian impact craters: implications for the rim formation of complex impact craters. J. Geophys. Res., Planets 121 (6), 1026–1053.

Turbet, M., Gillmann, C., Forget, F., Baudin, B., Palumbo, A., Head, J., Karatekin, O., 2020. The environmental effects of very large bolide impacts on early Mars explored with a hierarchy of numerical models. Icarus 335, 113419.

Van Rijn, L.C., 1984. Sediment transport, part I: bed load transport. J. Hydraul. Eng. 110 (10), 1431–1456.

Walder, J.S., O'Connor, J.E., 1997. Methods for predicting peak discharge of floods caused by failure of natural and constructed earthen dams. Water Resour. Res. 33 (10), 2337–2348.

Wang, C.-y., Manga, M., Hanna, J.C., 2006. Can freezing cause floods on Mars? Geophys. Res. Lett. 33 (20).

Warner, N., Gupta, S., Lin, S.-Y., Kim, J.-R., Muller, J.-P., Morley, J., 2010. Late Noachian to Hesperian climate change on Mars: evidence of episodic warming from transient crater lakes near Ares Vallis. J. Geophys. Res., Planets 115 (E6).

Whipple, K.X., Di Biase, R.A., Crosby, B.T., 2013. Bedrock rivers. In: Shroder, J., Wohl, E. (Eds.), Treatise on Geomorphology. Academic Press, San Diego, pp. 550–573.

Wilson, S.A., Howard, A.D., Moore, J.M., Grant, J.A., 2016. A cold-wet middle-latitude environment on Mars during the Hesperian-Amazonian transition: evidence from northern Arabia valleys and paleolakes: a late, cold, and wet climate on Mars. J. Geophys. Res., Planets 121 (9), 1667–1694. https://doi.org/10.1002/2016JE005052.

Supporting Information for "Overspilling small craters on a dry Mars: Insights from breach erosion modelling"

A. O. Warren[1], S. Holo[1], E. S. Kite[1], S. A. Wilson[2]

[1]University of Chicago, Chicago, IL, 6063, USA

[2]Center for Earth and Planetary Studies, National Air and Space Museum, Smithsonian Institution, 6th at Independence SW, Washington, DC, 20560, USA

Contents of this file

Introduction

Justification of model assumptions. Table of terrestrial analogue data used for model comparison. Figures illustrating comparisons of results for different sediment transport equations and critical bed shear stresses for sediment transport.

Text S1.

In our model derivation, we assume that pressure gradients in the flow diffuse on a shorter timescale than that of downwards erosion of the outflow valley (uniform flow), and that the timescales for the valley to erode by one grain diameter is smaller than the timescale for variations in flow depth (quasi-steady flow). The uniform flow assumption is justified because we assume that valley geometry does not change with downstream length. However, we can also demonstrate that these assumptions are justified by considering the relevant timescale for transport stage evolution. Eq. can be re-written in terms of T:

$$\frac{3}{2}\frac{Rd\tau_{*c}}{S}\frac{dT}{dt} = \frac{4Q_{in}}{\pi D^2} - \frac{32w_c g^{1/2}R^{5/3}d^{3/2}\tau_{*c}^{5/3}}{\pi D^2 S^{7/6}}T^{5/3} + \frac{8w_c}{w_v L}\sqrt{Rgd^3\tau_{*c}^3}(T-1)^{3/2} \tag{1}$$

This can be further re-written as:

$$\frac{3}{16}\frac{w_v L}{w_c}\sqrt{\frac{R}{gd\tau_{*c}}}\frac{dT}{dt} = \frac{w_v L}{2\pi D^2 w_c\sqrt{Rgd^3\tau_{*c}^3}} - \frac{4w_v L}{\pi D^2}\left(\frac{R}{S}\right)^{7/6}\tau_{*c}^{1/6}T^{5/3} + (T-1)^{3/2} \tag{2}$$

Where:

$$\frac{t}{t_*} = \frac{3}{16}\frac{w_v L}{w_c}\sqrt{\frac{R}{gd\tau_{*c}}} \tag{3}$$

Is the characteristic timescale for transport stage variation and t_* is dimensionless time. We can compare this to the characteristic timescale for a shallow-water gravity wave to travel up the valley:

$$t_w = \frac{L}{gH} \tag{4}$$

In our model, $\tau_{*c} < 1$, $S < 1$, and $H \geq d$, therefore the characteristic timescale for transport stage variation is much longer than the timescale for a pressure gradient to diffuse up the valley. This further justifies the uniform flow assumption.

To justify the quasi-steady assumption, we can consider the timescale t_d for erosion of the channel bed by one grain diameter d:

$$\frac{dB}{dt} \approx \frac{d}{t_d} \tag{5}$$

$$t_d = \frac{w_v L}{8 w_c \sqrt{Rgd\tau_{*c}}} \frac{1}{(T-1)^{3/2}} \tag{6}$$

Therefore, for all values of T where $T > \left(\frac{R}{S}\right)^{2/3} - 1$ ($T > 4$ for a typical pollywog slope), the quasi-steady flow assumption holds because the channel erodes on a shorter timescale than the transport stage changes, i.e., the transport stage remains approximately the same over the characteristic timescale for changes to the channel bed to occur. As T approaches 1, t_d approaches infinity, which violates the quasi-steady flow assumption because transport stage changes will outpace channel erosion. However, most erosion occurs shortly after breach erosion while T is high, where the quasi-steady flow assumption is valid, so we do not expect this assumption to strongly affect our results.

Table S1. Compilation of potential pollywog terrestrial analogue data.

Event Name	D (km)	L (km)	w_v (m)	S_{min}	S_{max}	z (m)	Reference
Nostetuko	2.5	2.5	100	0.19	0.83	40	(Clague & Evans, 2000)
Queen Bess	2.8	0.3	75	0.19	0.83	15	(Clague & Evans, 2000)
Tats Lake	0.113	0.5	25	0.19	0.83	9	(Clague & Evans, 2000)
Pinatubo	0.95	2	60	0.2	0.5	23	(Lagmay et al., 2007)
Paulina Creek	2.8	2.8	30	0.017	0.13	4.6	(Chitwood & Jensen, 2000)
Ram Creek, NZ	0.35	0.5	30	0.26	0.36	40	(Nash et al., 2008)
Bairaman, Papua New Guinea	3	2	400	0.2	0.3	70	(King et al., 1989)
El Chichon, Mexico	1.4	1	50	0.03	0.42	30	(Macías et al., 2004)
Khumbu Humal, Nepal	0.8	0.3	200	0.47	0.58	60	(Vuichard & Zimmermann, 1987)
La Josephina, Ecuador	1.9	1.9	200	0.25	0.45	40	(Plaza et al., 2011)
Poerua River, New Zealand	0.7	0.4	150	0.18	0.44	45	(Hancox et al., 2005)
Ventisquero Negro, Argentina	0.7	0.35	70	0.1	0.84	27	(Worni et al., 2012)
Tam Pokhari, Nepal	0.68	0.68	60	0.2	0.6	50	(Osti & Egashira, 2009)

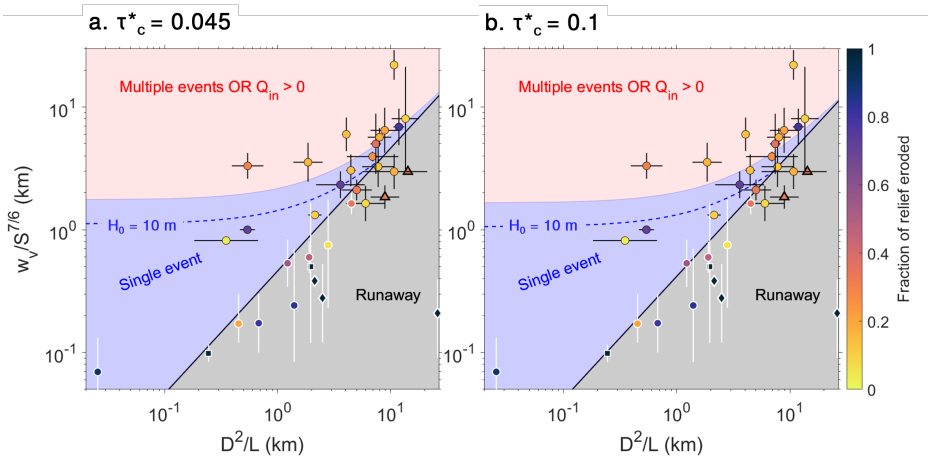

Figure S1. We compared the MPM bedload transport equation to 3 other bedload transport equations that are functions of bed shear stress and critical shear stress (Ribberink, 1998; Camenen & Larson, 2005; Parker et al., 1982) and found that MPM best matched our compilation of terrestrial data. All sediment transport equations predicted a runaway for the same two pollywogs, and Ribberink (1998) predicted an additional runaway case. a. Baseline model $\tau_{*c} = 0.045$, b. $\tau_{*c} = 0.1$. Symbology follows Fig. 3 in the main text. Blue shaded area indicates 95% confidence interval from 5,000 bootstraps for transition between an eroded breach being consistent with a single overspill event to requiring multiple events for initial flow depth $H_0 = 10$ m.

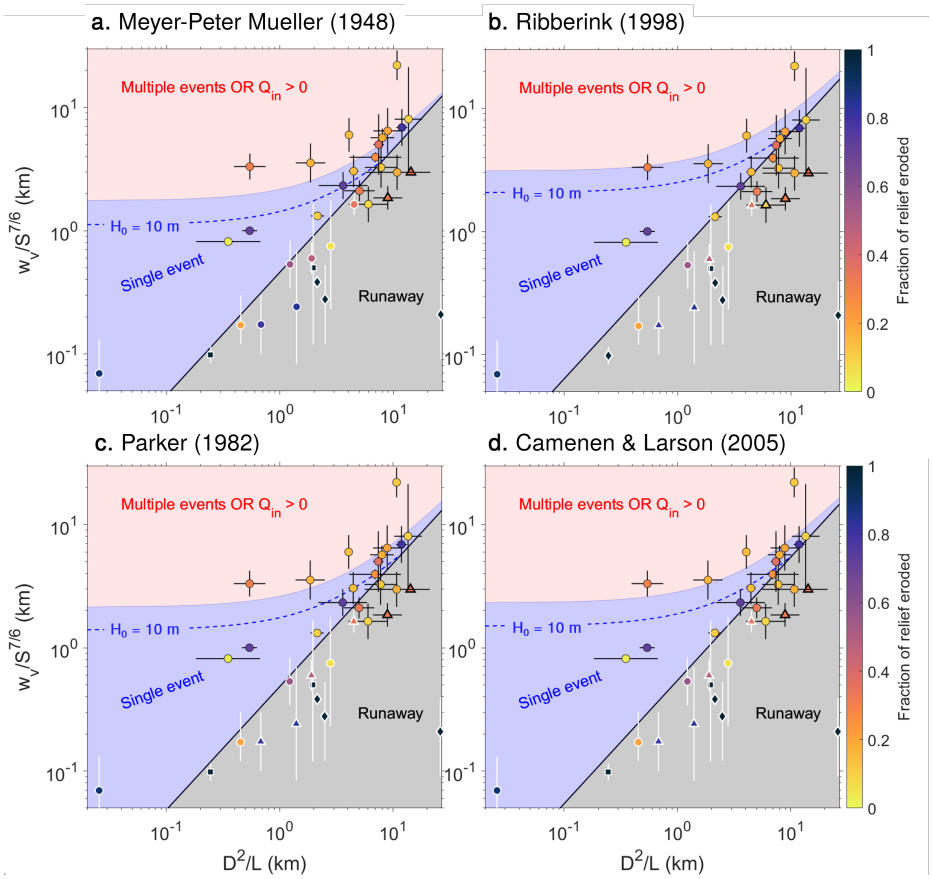

Figure S2. Comparison of different sediment transport equations to terrestrial data and pollywog measurements. Symbology follows Fig. 3 in the main text. a. Baseline model (Meyer-Peter & Mueller, 1948), b. Ribberink (1998), c. Parker et al. (1982), d. Camenen and Larson (2005). Blue shaded area indicates 95% confidence interval from 5,000 bootstraps for transition between an eroded breach being consistent with a single overspill event to requiring multiple events for initial flow depth $H_0 = 10$ m.

References

Camenen, B., & Larson, M. (2005). A general formula for non-cohesive bed load sediment transport. *Estuarine, Coastal and Shelf Science*, *63*(1-2), 249–260.

Chitwood, L. A., & Jensen, R. A. (2000). Large Prehistoric Flood Along Paulina Creek, Newberry Volcano, Oregon. *What's New at Newberry Volcano, Oregon: Guidebook for the Friends of the Pleistocene Eighth Annual Pacific Northwest Cell Field Trip*, 31–40.

Clague, J. J., & Evans, S. G. (2000). A review of catastrophic drainage of moraine-dammed lakes in British Columbia. *Quaternary Science Reviews*, *19*(17-18), 1763–1783.

Hancox, G. T., McSaveney, M. J., Manville, V. R., & Davies, T. R. (2005). The October 1999 Mt Adams rock avalanche and subsequent landslide dam-break flood and effects in Poerua River, Westland, New Zealand. *New Zealand Journal of Geology and Geophysics*, *48*(4), 683–705.

King, J., Loveday, I., & Schuster, R. L. (1989). The 1985 Bairaman landslide dam and resulting debris flow, Papua New Guinea. *Quarterly Journal of Engineering Geology and Hydrogeology*, *22*(4), 257–270.

Lagmay, A. M. F., Rodolfo, K. S., Siringan, F. P., Uy, H., Remotigue, C., Zamora, P., ... Ong, J. (2007, June). Geology and hazard implications of the Maraunot notch in the Pinatubo Caldera, Philippines. *Bulletin of Volcanology*, *69*(7), 797–809. doi: 10.1007/s00445-006-0110-5

Macías, J., Capra, L., Scott, K., Espíndola, J., García-Palomo, A., & Costa, J. (2004). The 26 May 1982 breakout flows derived from failure of a volcanic dam at El Chichón, Chiapas, Mexico. *Geological Society of America Bulletin*, *116*(1-2), 233–246.

Meyer-Peter, E., & Mueller, R. (1948). Formulas for bed-load transport. In *Iahsr 2nd*

meeting, stockholm, appendix 2.

Nash, T., Bell, D., Davies, T., & Nathan, S. (2008). Analysis of the formation and failure of Ram Creek landslide dam, South Island, New Zealand. *New Zealand journal of geology and geophysics*, *51*(3), 187–193.

Osti, R., & Egashira, S. (2009). Hydrodynamic characteristics of the Tam Pokhari Glacial Lake outburst flood in the Mt. Everest region, Nepal. *Hydrological Processes: An International Journal*, *23*(20), 2943–2955.

Parker, G., Klingeman, P. C., & McLean, D. G. (1982). Bedload and size distribution in paved gravel-bed streams. *Journal of the Hydraulics Division-Asce*, *108*(HY4), 544–571.

Plaza, G., Zevallos, O., & Cadier, É. (2011). La Josefina Landslide Dam and Its Catastrophic Breaching in the Andean Region of Ecuador. In *Natural and artificial rockslide dams* (pp. 389–406). Springer.

Ribberink, J. S. (1998). Bed-load transport for steady flows and unsteady oscillatory flows. *Coastal Engineering*, *34*(1-2), 59–82.

Vuichard, D., & Zimmermann, M. (1987). The 1985 catastrophic drainage of a moraine-dammed lake, Khumbu Himal, Nepal: cause and consequences. *Mountain Research and Development*, 91–110.

Worni, R., Stoffel, M., Huggel, C., Volz, C., Casteller, A., & Luckman, B. (2012). Analysis and dynamic modeling of a moraine failure and glacier lake outburst flood at Ventisquero Negro, Patagonian Andes (Argentina). *Journal of Hydrology*, *444*, 134–145.